JOURNAL OF AIRCRAFT
Vol. 45, No. 3, May–June 2008

Semi-Active Magnetorheological Helicopter Crew Seat Suspension for Vibration Isolation

Gregory J. Hiemenz,* Wei Hu,† and Norman M. Wereley‡
University of Maryland, College Park, Maryland 20742

DOI: 10.2514/1.32736

This study explores the use of magnetorheological dampers in a semi-active seat suspension system for helicopter crew seats to enhance occupant comfort. Key concepts in designing a magnetorheological seat suspension system to isolate the occupant from rotorcraft vibration are identified. Using these design concepts, a magnetorheological damper is designed, fabricated, and retrofitted into a tactical SH-60 Seahawk crew seat. This magnetorheological damper is implemented in series with the existing fixed load energy absorbers such that the crashworthiness capability of the seat is not impaired. Semi-active control is implemented and performance is evaluated both analytically and experimentally. Experimental test results have shown that this system reduced the dominant rotor-induced vertical vibration (4 per rev) transmitted to a 50th percentile male aviator by 76%, which is a 61–70% improvement over the unmodified SH-60 crew seat depending upon whether a soft seat cushion is used. Furthermore, these experimental tests also show that this system significantly reduces vertically induced seat rocking that occurs as a result of an offset center of gravity in the crew seat design.

Nomenclature

C_o	=	off-state viscous damping
C_p	=	postyield viscous damping
C_{sky}	=	skyhook control gain
d	=	offset in center of gravity of the stroking portion of the seat
F_{MR}	=	total MR damper force
F_{on}	=	maximum on-state total MR damper force at piston velocity v
F_{sky}	=	skyhook control force
F_y	=	MR damper yield force
I	=	current applied to MR damper
M	=	effective occupied seat mass
v	=	piston velocity (relative velocity between seat and floor)
v_s	=	absolute velocity of seat
ζ	=	off-state viscous damping ratio
ζ_{sky}	=	equivalent viscous damping ratio for skyhook control
ω_n	=	fundamental resonance of seat suspension system
1P	=	1/rev or 1 per rev, the basic helicopter rotation frequency or rotor rpm
4P	=	4/rev or 4 per rev, blade passing frequency for 4-bladed helicopter
8P	=	8/rev or 8 per rev, second harmonic of blade passing frequency for 4-bladed helicopter

I. Introduction

WHOLE body vibration (WBV) has become an increasingly significant area of concern in helicopter seat design. Military studies and hazard reports have shown that back pain and spinal abnormalities are prevalent among helicopter pilots [1]. Such pain has been identified as extreme localized pain and becomes chronic as rotary wing flight exposure increases [1,2]. Hazard reports have indicated that such pain in the lumbar region, buttocks, and legs begins 2–4 h into the flight and increases with time [2]. Growing operational demands and evolving military strategies have significantly increased the frequency of extended duration missions (>6 h) [2], exacerbating the problem. Studies have also shown that such physical discomfort leads to inattention and distraction, contributing to a loss of situational awareness and poor decision making in both training and missions [2,3].

Current seating systems are designed primarily to meet crashworthiness requirements rather than vibration isolation [2,4]. They employ crashworthy fixed load energy absorbers (FLEAs) to minimize the potential for occupant spinal and pelvic injuries during harsh vertical or crash landings of these aircraft and increase the chances of occupant survival during these events [5,6]. These FLEAs, however, will not stroke until a tuned load threshold is reached and therefore act as a stiff link between the seat and the floor during normal rotorcraft vibration. Because of this, these systems provide no isolation to rotor-induced vibration [4]. Although crash safety is a critical issue, pilot fatigue and chronic health problems as well as reduced mission effectiveness are also serious concerns [2].

A number of researchers have been motivated to study innovative seat suspensions showing improved vibration attenuation performance controlling stiffness and/or damping. Choi et al. successfully used both electrorheological (ER) and magnetorheological (MR) seat suspensions to attenuate vibration in commercial vehicles using skyhook and sliding mode control algorithms [7,8]. Park and Jeon devised a Lyapunov-based robust control algorithm that compensates for actuator time delay and evaluated its performance in controlling vibration using an MR seat suspension [9]. McManus et al. used MR seat suspensions to reduce the frequency and severity of end-stop impacts, showing favorable performance in both attenuating end-stop impact and reducing vibration exposure [10]. Finally, Choi and Wereley evaluated the biodynamic response of the seated human occupant protected by a controlled MR rotorcraft seat suspension to both sinusoidal vibration and crash loads, and compared these results with passive hydraulic seat suspensions [5].

MR dampers are attractive for rotorcraft seat suspension systems as they are capable of achieving what is effectively a continuously adjustable device [11] and, in combination with a real-time feedback controller, can adapt to occupant weight and respond to changing excitation levels and frequencies. They are also attractive because of

Presented as Paper 1722 at the 15th AIAA/ASME/AHS Adaptive Structures Conference, Honolulu, HI, 23–26 April 2007; received 10 June 2007; revision received 5 August 2007; accepted for publication 15 October 2007.

*Graduate Research Assistant, Smart Structures Laboratory, Department of Aerospace Engineering, 3181 Martin Hall. Member AIAA.

†Assistant Research Scientist, Smart Structures Laboratory, Department of Aerospace Engineering, 3181 Martin Hall. Member AIAA.

‡Professor, Smart Structures Laboratory, Department of Aerospace Engineering, 3180 Martin Hall. Associate Fellow AIAA.

their low power draw, high mechanical reliability, and the fact that they will operate as a conventional hydraulic damper in a fail-safe condition when there is a loss in power. Recent studies have shown that MR dampers have the capability of achieving both enhanced crashworthiness and vibration isolation using the same device, which can be very attractive from a systems integration standpoint [4]. Investigation has shown, however, that using conventional MR technology, designing for the dual goals of adaptive crashworthiness and vibration isolation tends to lead to undesirably large devices that complicate the retrofit into existing rotorcraft seats [4]. This paper investigates an MR seat suspension optimized solely for vibration isolation of an unarmored Navy SH-60 Seahawk crew seat. This MR seat suspension is easily retrofitted into the crew seat such that crash safety is preserved, while the occupant is isolated from harmful vibrations during normal operations.

II. MR Seat Suspension Design Principles

For vibration isolation, it is advantageous to tune the fundamental resonance of the seat suspension system as far below excitation frequencies as possible to take advantage of the resulting low transmissibility. As shown in the nondimensionalized frequency response for a based-excited single-degree-of-freedom (SDOF) system (Fig. 1), when the excitation frequencies are greater than those of the fundamental resonant peak, the transmissibility of the base excitation is less than one, thus isolating the occupant from floor vibrations. In this figure, the transmissibility is plotted for different values of the viscous damping ratios, ζ. For isolation of these higher excitation frequencies, the best performance is achieved when ζ is very small, meaning low viscous damping. As viscous damping is increased, high-frequency transmissibility increases. It is therefore desirable to have the viscous damping component as low as possible to maintain desirable isolation of the high-frequency excitation.

Although it is desirable to tune the fundamental resonance of the suspension system to be as low as possible, there are practical limitations. Line-of-sight issues may arise if the tuned spring stiffness is too low and the static deflection is large. For this study, a maximum static deflection of 13 mm for the 95th percentile male aviator (96.1 kg [12]) is assumed. It is also assumed that 29% of the occupant's weight is supported by the floor (legs) [13], that there is 13.6 kg of body worn equipment, and that the stroking seat mass is 11.5 kg. Using these design parameters, the resulting design spring stiffness is 70 N/mm, setting the fundamental resonance at 4.4 Hz for the 95th male aviator. Because it is possible that this resonance may be excited by the rotor 1/rev (1P) vibrations, occupant motion, and/or turbulence, utilization of semi-active control is very beneficial. The objective of semi-active control is to combine the resonance response of a highly damped system with a high-frequency response of a lightly damped system as illustrated in Fig. 2.

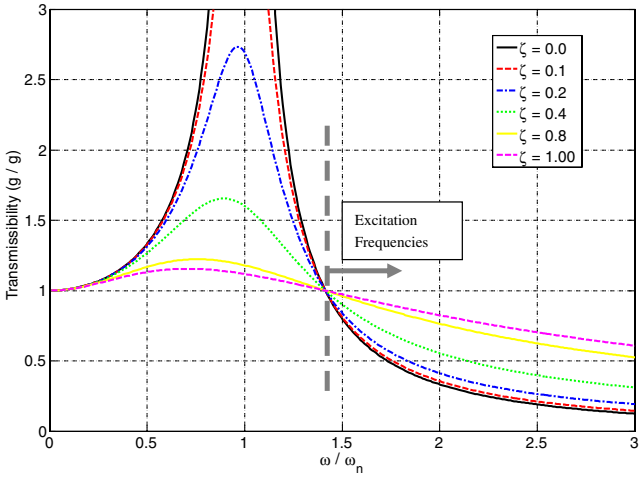

Fig. 1 Transmissibility for SDOF system to base excitation for varying viscous damping levels.

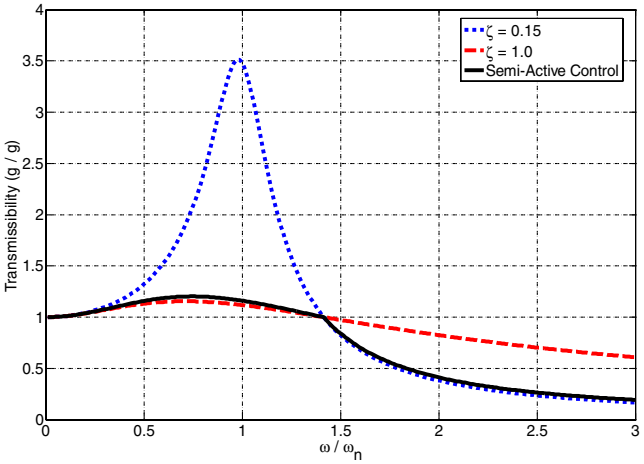

Fig. 2 Illustration of semi-active control objective.

To apply this design philosophy to MR dampers, the most simple and widely used force model for MR dampers, the Bingham-plastic model, is used,

$$F_{\mathrm{MR}} = C_p v + F_y \mathrm{sign}(v) \tag{1}$$

Here, F_{MR} is the total force dissipated by the MR damper, F_y is the controllable yield force, C_p is the postyield viscous damping, and v is the piston velocity. When no electric current is applied, the postyield viscous damping is known as the off-state viscous damping [i.e., $C_p(0) = C_o$]. In this off-state condition, the yield force of an MR damper is ideally zero and, thus, the viscous damping ratio in the off-state is simply given by

$$\zeta = \frac{C_o}{2\omega_n M} \tag{2}$$

where M is the effective suspended mass (seat+percentage of occupant), and ω_n is the tuned fundamental resonance of the system.

To further quantify the effect of an MR damper's off-state viscous damping component on vibration isolation performance, the above SDOF system is assumed for an MR seat suspension in an unarmored SH-60 Seahawk crew seat. Figure 3 shows this crew seat as produced by Armor Holdings, Inc. The SH-60 has four blades and a main rotor frequency of 4.3 Hz. Primary rotor-induced vibrations, therefore, occur at the blade passing frequency (17.2 Hz—4 per rev) and harmonics thereof (34.4 Hz—8 per rev, etc.) [14]. Using this SDOF assumption, Fig. 4 plots the isolation level (in percent reduction) that an MR seat suspension can provide for a 0.2 g amplitude, 4 per rev (4P) vertical floor excitation as a function of the off-state viscous

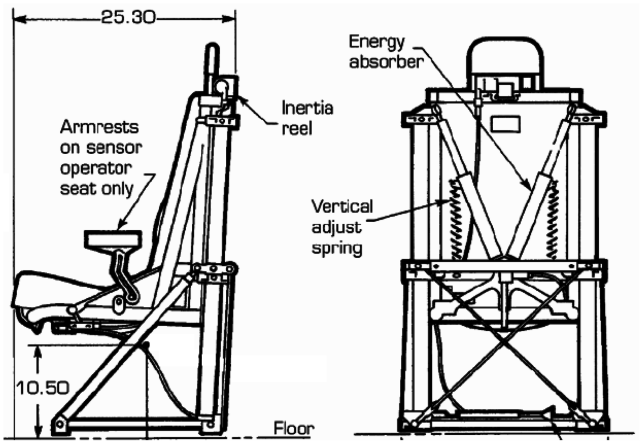

Fig. 3 Unarmored SH-60 Seahawk crew seat produced by armor holdings.

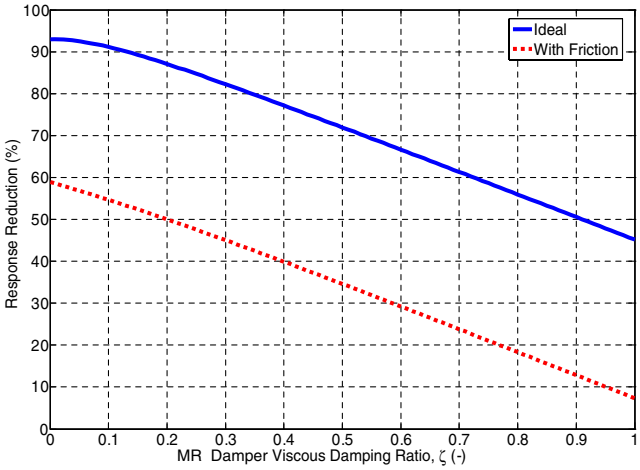

Fig. 4 Vibration reduction because of 0.2-g amplitude 4P floor excitation vs MR damper viscous damping ratio.

damping ratio. It can be seen that for an ideal system, the MR suspension provides 93% vibration reduction assuming zero off-state viscous damping. As the off-state viscous damping ratio is increased, this vibration isolation performance drops significantly, down to 45% reduction for $\zeta = 1.0$. In such a system, however, this vibration performance can be degraded because of friction in the system. Friction in MR dampers is typically due to contact in rod seals and piston rings and can range from 20 to 200 N depending upon the damper design. MR dampers designed for high fluid pressures (e.g., high piston velocities and high force) typically have higher friction because of the increased fluid sealing required. The dashed line in Fig. 4 shows the response reduction assuming 80 N of friction in the system. It can be seen that isolation performance now ranges from 60% reduction down to 8% reduction. This further emphasizes the need to maintain the off-state viscous damping ratio as low as possible and illustrates the importance of keeping system friction as low as possible.

III. Designing MR Dampers for Vibration Isolation

As discussed above, the off-state viscous damping ratio is a key parameter in vibration isolation performance. When designing for vibration isolation, the viscous damping ratio, therefore, becomes an important design parameter. Up to this point, however, the damping ratio has not been considered in MR damper design strategies. To address this, we can combine Eq. (2) with that for MR damper's dynamic range:

$$D = \frac{F_{\text{on}}}{C_o v} \tag{3}$$

$$= \frac{F_{\text{on}}}{2\zeta\omega_n M v} \tag{4}$$

Using this equation, one can determine the necessary dynamic range based on system properties (resonant frequency, stroking mass) and desired vibration isolation performance. Plots such as Fig. 4 can be used to aid in the selection of the viscous damping ratio. This dynamic range can then be used as a design parameter in MR damper design strategies such as that proposed by Mao et al. [15].

For effective semi-active control, the off-state viscous damping ratio should ideally be less than 0.2. Beyond this level, there begins to be a significant loss in high-frequency isolation performance, as shown in Fig. 1. For this study, a viscous damping ratio of 0.15 is chosen as the desired design parameter. Using Eq. (4) and the seat resonant frequency and effective seat mass for a 95th male aviator discussed previously, this gives an off-state viscous damping ratio, C_o, of 0.77 N · s/mm. Assuming two MR dampers per seat, this gives a viscous damping ratio of 0.38 N · s/mm per damper.

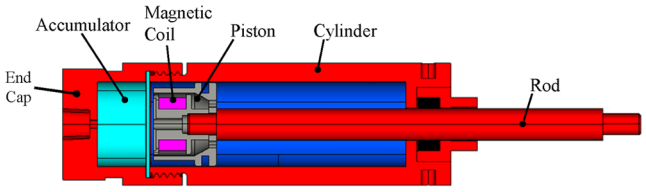

Fig. 5 MR damper optimized for vibration isolation.

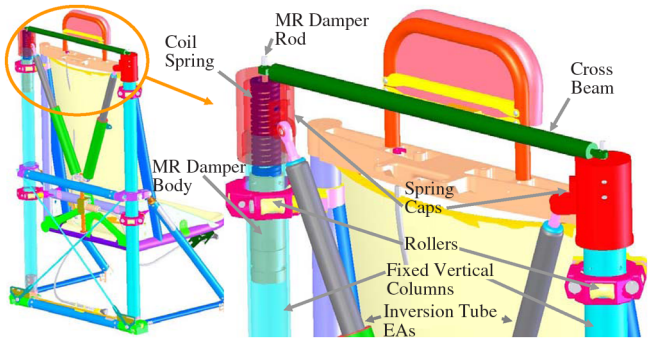

Fig. 6 MR dampers retrofitted into SH-60 crew seat in series with inversion-tube FLEAs.

To determine dynamic range, the maximum total MR damper force, F_{on}, necessary for resonance mitigation must also be determined. From Fig. 2, the peak transmissibility at resonance for viscous damping ratios of 0.15 and 1.0 are 3.51 and 1.16, respectively. The difference between these transmissibilities (2.35) multiplied by the effective occupied seat mass, M, and the maximum expected vibration at the floor of the cockpit (assumed to be 0.2 g for this study) gives the additional damping force necessary to mitigate the resonance to be 430 N. This value was further verified using a simple SDOF simulation where the control force was varied using the skyhook control algorithm [16] where the rate-feedback gain was set to be the viscous damping calculated for $\zeta = 1$ (as discussed in Sec. V). In this simulation, the relative velocity between the base and the effective mass (the piston velocity) at resonance was determined to be 30 mm/s.

For two MR dampers per seat, the designed field-off MR damper force, F_{off}, is 11 N (0.38 N · s/mm × 30 mm/s), the necessary field-on MR damper force, F_{on}, is then 226 N (F_{off} + 430 N ÷ 2), and the dynamic range, D, is 19.6 [per Eq. (3)] at a piston velocity of 30 mm/s. With these key parameters, the design strategy discussed in [15] was then used to design the MR damper depicted in Fig. 5. This design has a piston diameter of 25 mm, and the MR valve has an annular duct with a gap distance of 0.35 mm and an active length of 2.1 mm. The total stroke capability is 65 mm, which allows for vibration magnitudes up to 2.5 g. These MR dampers have a 38-mm outer diameter, only a 114-mm body length, and have a prototype weight of 1 kg each (using a steel body). Estimated production weight for this MR damper is 0.5 kg each (assuming a weight-optimized aluminum body).

Although these MR dampers significantly reduce vibration, they are not capable of mitigating shock loads. These MR dampers, therefore, must be integrated into the crew seat in such a way that they do not interfere with the operation of the FLEAs. One method of doing this is to couple them in series with the existing inversion-tube FLEAs, as shown in Fig. 6.[§] In this configuration, the MR dampers are mounted within the two fixed vertical columns to which the seat rollers attach. The MR damper connects to the inversion-tube energy absorbers via a spring and spring cap. The opposite ends of the FLEAs are then attached to the base of the stroking seat. This allows for the seat to stroke under normal operating vibratory conditions when the force levels are not high enough to stroke the FLEAs. At a tuned base input level (2 g), the spring cap bottoms out on the top of

[§]Patent pending.

the fixed vertical column and the MR damper is taken out of the load path. This allows the inversion-tube FLEAs to operate as originally designed when a crash/shock event occurs, with the FLEA load being transmitted directly to the fixed vertical columns. Finally, a crossbeam has been added which spans between the two spring caps. The purpose of this crossbeam is to react the lateral component of the loads transmitted through the FLEAs (and moments generated by them) against one another, thereby reducing friction in the system. This retrofit requires only minor modifications to the fixed vertical columns (remove old FLEA attachment points and add new MR damper mounting fixtures) and provides the ability to effectively isolate vibration while preserving crashworthy capabilities.

IV. MR Damper Characterization

Before implementing semi-active control, the MR dampers had to be tested to verify their performance and characterize their dynamic parameters. Dynamic testing under steady-state sinusoidal loading was performed using an MTS® 810 24.466 kN (5000 lb) servo-hydraulic material testing machine. A displacement linear variable differential transformer (LVDT) sensor was used for displacement measurement and a load cell measured the force. Fittings were designed to hold the damper securely in place. A dc power supply was used to provide current control during testing and was connected to the magnetic coil leads. The normal range of the applied current was between 0 and 1.5 A, and the maximum applied voltage was 10 V dc.

The MR dampers were tested over a range of realistic frequencies (from quasi static to 4/rev of rotor rpm) and amplitudes ranging from 0.1 to 0.4 in. At each of these 11 combinations of frequency and amplitude, the MR damper was energized with 0, 0.25, 0.5, 0.75, 1.0, and 1.5 A of applied current. All tests were performed at room temperature (25°C). Force vs displacement data was recorded for each of these 66 cases. Figure 7 shows example raw force vs displacement data taken in these tests for this MR damper design. From these data, the force vs velocity curves was also generated. Sample force vs velocity curves is shown in Fig. 8.

The goal of MR damper characterization was to determine the parameters C_p and F_y of the Bingham-plastic MR damper force model [Eq. (1)] as a function of current applied to the magnetic coil. As an example, Fig. 9 plots a fitted Bingham-plastic model against the results for 1-Hz, 0.2-in. amplitude excitation with the solid lines representing the Bingham-plastic approximation. It can be seen that the off-state MR damper yield force, $F_y(0A)$, is nonzero (36 N) because of friction at the rod seal and piston ring. This Bingham-plastic force model approximation was made for each MR damper test case. The resulting yield forces and postyield viscous damping were plotted in Figs. 10 and 11, respectively, against the current applied to the magnetic coil.

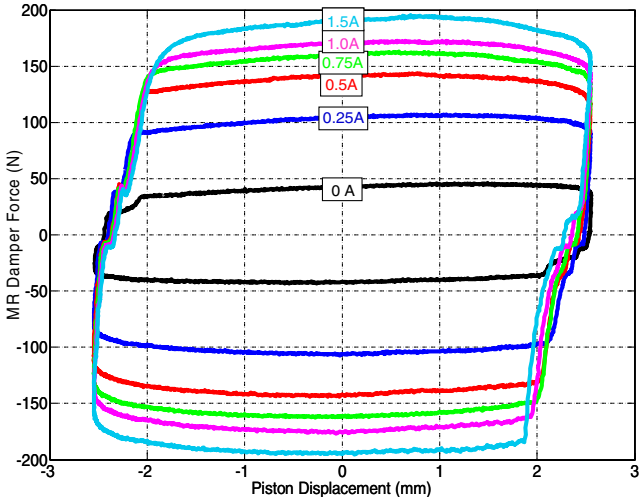

Fig. 7 Raw force vs displacement data for 1 Hz, 0.1-in. amplitude excitation.

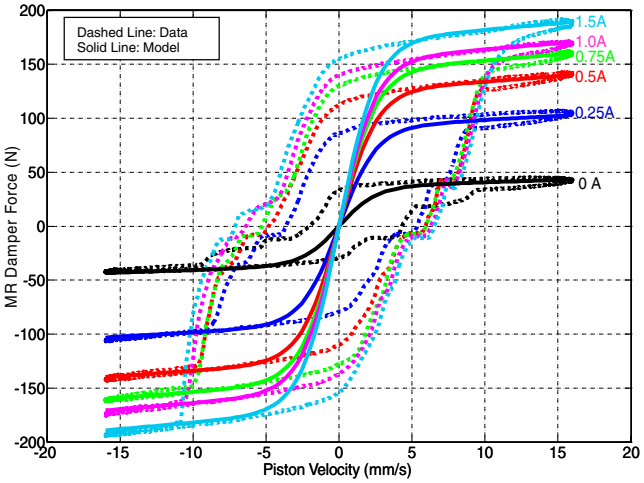

Fig. 8 Force vs piston velocity data for 1 Hz, 0.1-in. amplitude excitation.

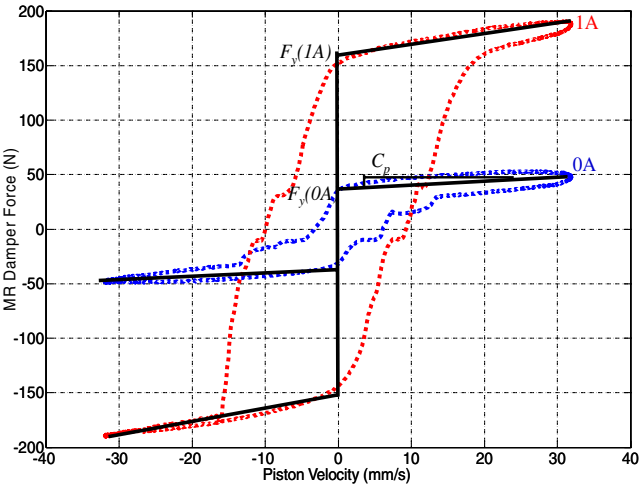

Fig. 9 Fitting Bingham-plastic model to MR damper results for 1-Hz, 0.2-in. amplitude excitation.

In these plots, the trends can be fitted with cubic polynomial functions:

$$F_y = 65I^3 - 218I^2 + 269I + 36 \tag{5}$$

$$C_p = 0.37I^3 - 1.28I^2 + 1.59I + 0.45 \tag{6}$$

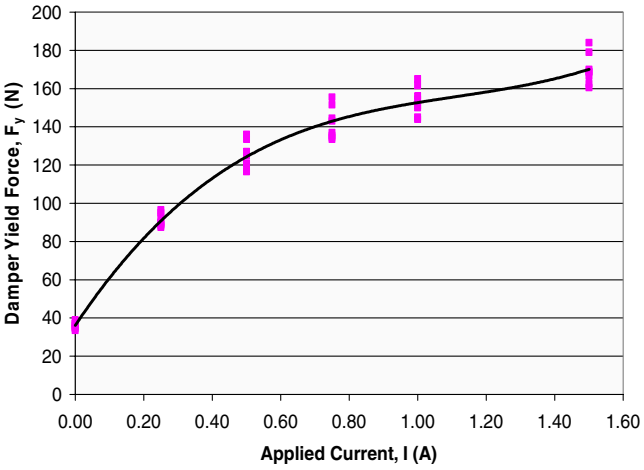

Fig. 10 Fitting cubic function to yield force, F_y, vs applied current.

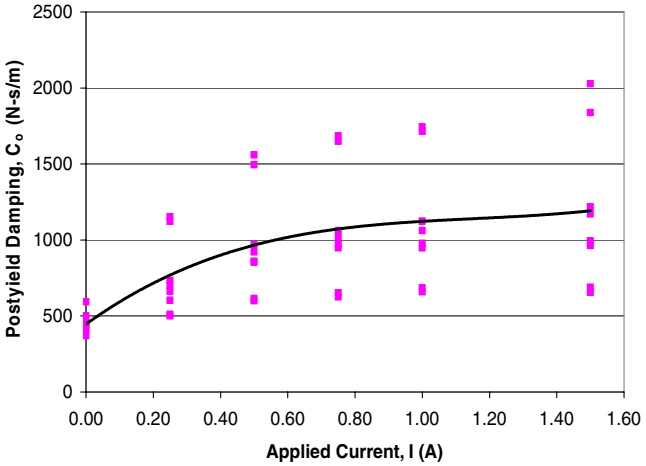

Fig. 11 Fitting a cubic function to postyield damping, C_p, vs applied current.

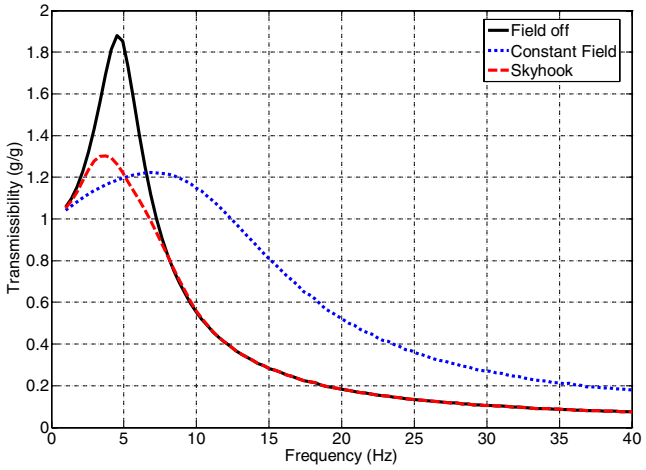

Fig. 12 SDOF skyhook control performance prediction for 50th percentile male crew seat occupant.

where I is the applied current (in A) and the C_o and F_y are in units of N · s/mm and N, respectively. By solving these cubic functions, a semi-active controller can calculate the amount of current that needs to be applied for a given desired force and measured piston velocity. The solid lines in Fig. 8 show this model plotted against the test data. In these plots, the signum function in the Bingham-plastic force model [Eq. (1)] is approximated using a hypertangent function as shown in Eq. (7) to give a smooth transition through the yield region at low speed. As shown in Fig. 8, the MR damper yield force and postyield damping are well represented using this model:

$$F_{\mathrm{MR}} = C_p v + F_y \tanh\left(\frac{v}{0.1}\right) \tag{7}$$

V. Semi-Active Control

In 1974, Karnopp et al. [16] introduced a simple, yet effective vibration isolation strategy that is realized by a fictitious damper connecting between the sprung mass and the stationary sky. In this control scheme, known as skyhook control, the damper exerts a force tending to reduce the *absolute* velocity of the sprung mass. This differs from conventional dampers, which exert forces that tend to reduce the *relative* velocity between the sprung mass and the base. Although conventional dampers reduce the resonant response, it is at the cost of increased high-frequency response. This is because, at high-frequency inputs, they tend to stiffen the suspension when a soft suspension is desired. The skyhook algorithm, however, effectively achieves a combination of resonance damping and high-frequency isolation [16]. For an MR damper installed in place of a conventional damper, this control strategy essentially turns the damper on to the desired force (linearly proportional to sprung mass absolute velocity) when it is the same sign as relative velocity and turns the damper off when they are opposite, ensuring that the force is always dissipative:

$$F_{\mathrm{sky}} = \begin{cases} C_{\mathrm{sky}} v_s, & \text{if } v_s \cdot v \geq 0 \\ 0 & \text{if } v_s \cdot v < 0 \end{cases} \tag{8}$$

For this study, the skyhook control gain, C_{sky}, was determined by assuming critical equivalent viscous damping at the resonance:

$$C_{\mathrm{sky}} = 2\zeta_{\mathrm{sky}} \omega_n M \tag{9}$$

where $\zeta_{\mathrm{sky}} = 1.0$.

Using a simple SDOF simulation, the semi-active control performance for the MR suspension can be predicted. Figure 12 shows the simulated SDOF frequency response for three cases: 1) unenergized MR dampers (field off), 2) constant maximum energized MR dampers (constant field), and 3) skyhook control. This particular case is for the 50th percentile male aviator (77.5 kg) and the suspension properties described previously. In this simulation, the off-state viscous damping ratio, friction force, and maximum yield force determined from the MR damper testing are used. It can be seen that in the field-off case, there is a high resonant peak around 4.5 Hz. In the constant field case, this resonance is well damped, but the high-frequency isolation is very poor. The skyhook control case, however, combines resonance damping with desirable high-frequency isolation performance. This simulation estimates that the MR suspension with skyhook control will reduce the floor vibrations transmitted to the seat by 77% and 91% for the 4P (blade passing) and 8P (first blade passing harmonic) frequencies, respectively.

VI. Experimental Setup

The retrofitted SH-60 crew seat was installed into the Vertical Axis Shock and Vibration Test Stand at the University of Maryland Smart Structures Laboratory (Fig. 13). This test facility has provisions for simulating up to 21 ft/s sink rate crashes as well as floor vibration via a MTS model 242 portable hydraulic actuator. Triaxial accelerometers were mounted to the base of the trolley to record input motion as well as on the seat pan and seat back to record

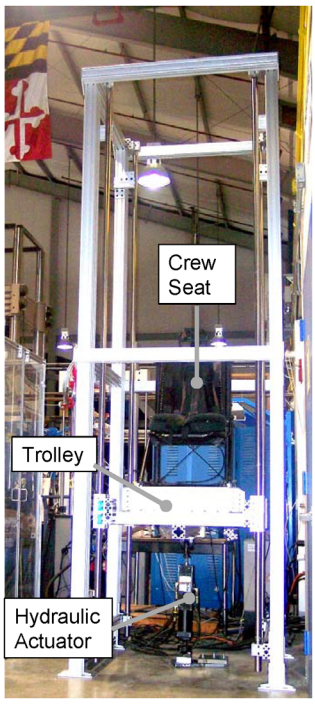

Fig. 13 Crew seat installed in vertical axis shock and vibration test stand.

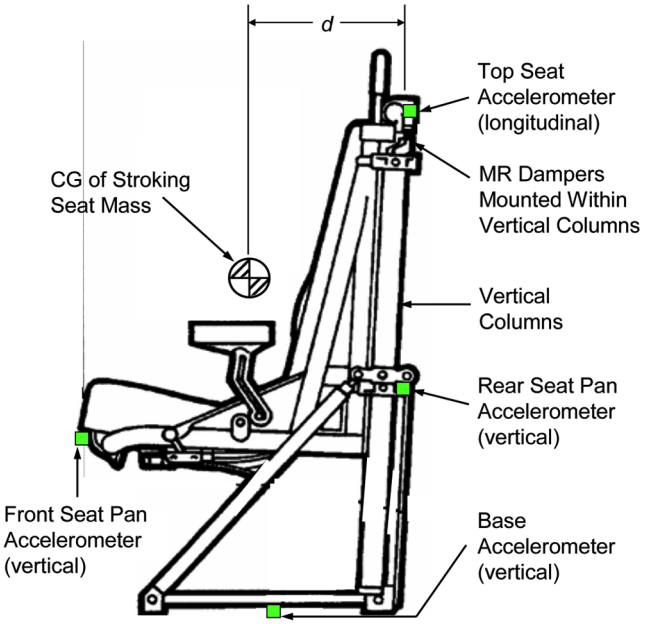

Fig. 14 Accelerometer placement on seat.

resulting seat motion as shown in Fig. 14. This crew seat design is known to be prone to vertically induced longitudinal rocking because of the offset, *d*, between the center of gravity (CG) of the stroking seat and where it attaches to the fixed vertical columns as shown in Fig. 14. The experimental accelerometer placement allows for measurement of both pure vertical vibrations as well as this rocking motion of the seat.

These accelerometers were connected to both a dSpace Rapid Prototyping System (for control) and Siglab Data Acquisition System (to collect frequency response data) via the accelerometer signal conditioner. The seat trolley was vibrated using the MTS model 242 portable hydraulic actuator. This hydraulic actuator was controlled using the Siglab system to provide a sinusoidal base excitation with constant input acceleration amplitude of 0.2 g while sweeping from 2 to 20 Hz.

A MATLAB Simulink control diagram which implemented the aforementioned skyhook control algorithm was uploaded to the dSpace system. Accelerometer signals were then fed to the accelerometer signal conditioner and then into the dSpace controller. The dSpace controller then determined the desired electric current to be applied to the MR dampers (based upon the control algorithm, measured accelerometer signals, and the MR damper model) and then supplied this control current to the MR dampers via a current amplifier.

The tests used "dead weight" in the seat. A combination of steel and/or sand bag weights were attached to the seat to simulate the *effective* mass for 5th percentile female (103 lb), 50th percentile male (151 lb), and 95th percentile male (183 lb) occupants with equipment (30 lb) [12]. Four sine sweep tests were performed for each of these three occupant weights: 1) unmodified SH-60 crew seat, 2) field off (no magnetic field applied to MR damper), 3) constant 0.5 A (damper on, but uncontrolled with a constant magnetic field of 0.5 A), and 4) skyhook control. In addition to varying occupant weight, two additional sets of sine sweeps were performed for the 50th percentile male to examine the sensitivity of the cushion and of higher (0.4 g) input acceleration, respectively. For each of these tests, acceleration data from the seat and base were recorded for generation of transmissibility plots (frequency response) in the next section.

VII. Experimental Results and Discussion

Figure 15 shows the rear seat pan transmissibility data measured from the Siglab data acquisition system for the 50th percentile male and without the use of a soft cushion. It can be seen in this plot that, for the unmodified seat, there was a large resonance seen between 6

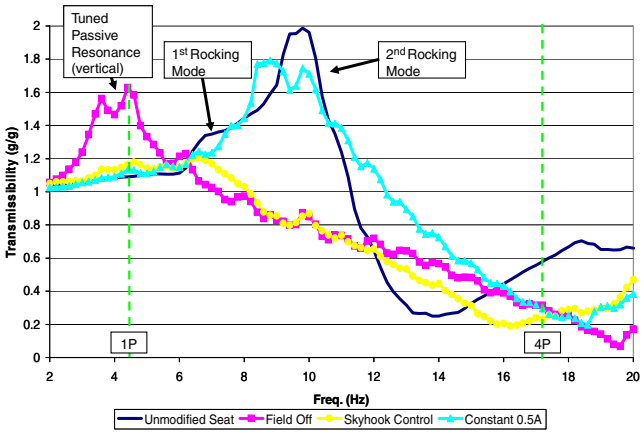

Fig. 15 Rear seat pan vertical transmissibility for 50th percentile male, 0.2 g excitation.

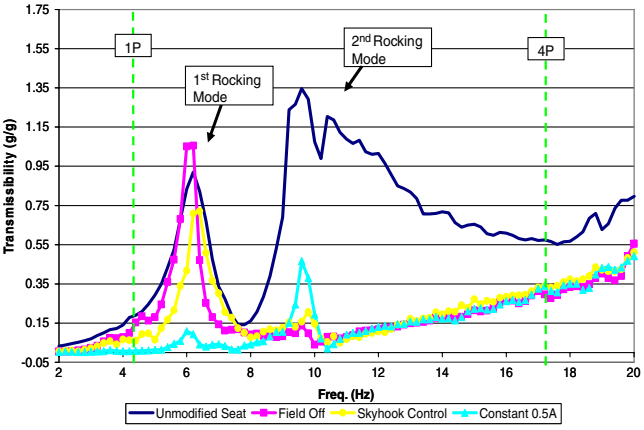

Fig. 16 Seat top longitudinal coupling transmissibility for 50th percentile male, 0.2 g excitation.

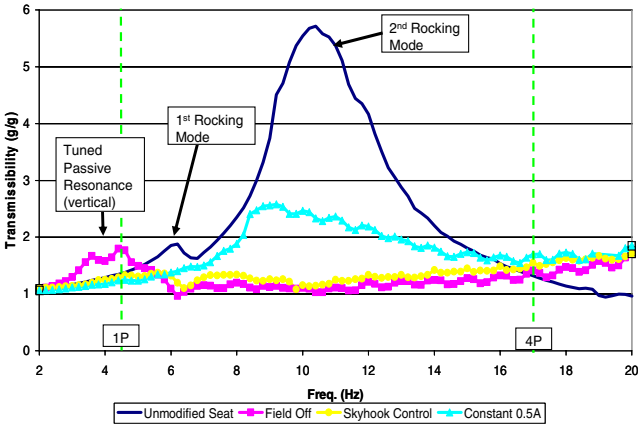

Fig. 17 Front seat pan vertical transmissibility for 50th percentile male, 0.2 g excitation.

and 11 Hz. Figures 16 and 17, however, show that this was actually the result of two separate rocking modes. Besides observations during the test, this was evidenced by the fact that there is coupling between the seat top longitudinal acceleration and the base (Fig. 16). This coupling is due to the fact that the occupant CG is forward of the fixed vertical columns, to which the seat is mounted (Fig. 14), and thus creates a moment under vertical base excitation. The levels of these two rocking modes and visual observations during the test suggest that the first of these two rocking modes (at 6 Hz) is a rigid body mode due to the large clearances between the seat rollers and the columns. The second rocking mode, however, was due to the seat

pan bending down away from the seat back, which explains why the front seat pan vertical transmissibility (Fig. 17) was very high at the second rocking modal frequency.

Next, the effects of installing the suspension system were examined. Starting with the unenergized (field-off) system, it can be seen in Fig. 16 that the spring and damper added the tuned resonance around 4 Hz. While this increases the transmissibility at the rotor rpm (1P), the rocking modes and the blade passage frequency (4P), where the majority of the rotor-induced vibration and associated discomfort occurs, were significantly reduced. The fact that the rocking modes were also reduced is further evidenced in Figs. 15 and 17. The rocking modes were reduced because the vertical transmissibility is reduced, thus reducing the moment due to the CG offset discussed previously.

The effect of energizing the system was then examined. At a constant applied current of 0.5 A, the tuned passive resonance was nearly eliminated and the rocking modes were again observed (albeit to a slightly lesser magnitude). This is because the high MR constant damper force tends to lock up the damper, causing it to behave similarly to the unmodified seat.

Finally, it can be seen in these plots that when the semi-active (skyhook) control was implemented, the resonance was significantly reduced while maintaining the desirable high-frequency isolation performance of the field-off system. Figure 16 shows that the controlled system reduces the 4P vertical vibration transmitted to the occupant by 77%, which is 61% better than the original seat. It should be noted that the 77% reduction of the vertical 4P floor vibration matches the predictions made in Sec. V. This shows that, while the SDOF system does not capture the complex rocking dynamics of the seat, it can give a very good estimate of vertical attenuation and is useful for system design. Additionally, Figs. 15 and 17 show seat top longitudinal and front seat pan vertical transmissibilities at the second rocking mode are reduced by 85 and 80%, respectively. These reductions come at a slight sacrifice to transmissibility at the 1P frequency (8% increase) which is acceptable because these frequencies are rarely experienced during typical helicopter vibration (only if there is a very significant blade imbalance).

Figure 18 shows example time history data taken while the controlled system was near its fundamental vertical resonance. The top plot in this figure shows the absolute seat velocity measured versus the relative velocity measured between the seat and the floor. The middle plot in this figure shows how the skyhook control force is proportional to the absolute velocity, except for when it is set to zero because it is the opposite sign of the relative velocity [per Eq. (8)]. The bottom plot in Fig. 18 shows the electric current applied to the MR dampers which is calculated by the controller by combing Eqs. (1), (5), and (6), and solving for electric current, I, given the desired control force, F_{sky}, and relative (piston) velocity, v.

The effect of varying occupant weight was also considered. Figure 19 shows the rear seat pan vertical transmissibility for the fifth

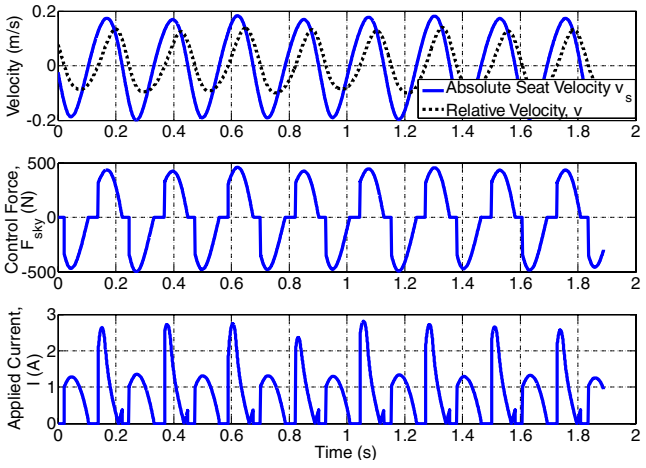

Fig. 18 Time history data near resonance, 50th percentile male, 0.2 g amplitude floor excitation.

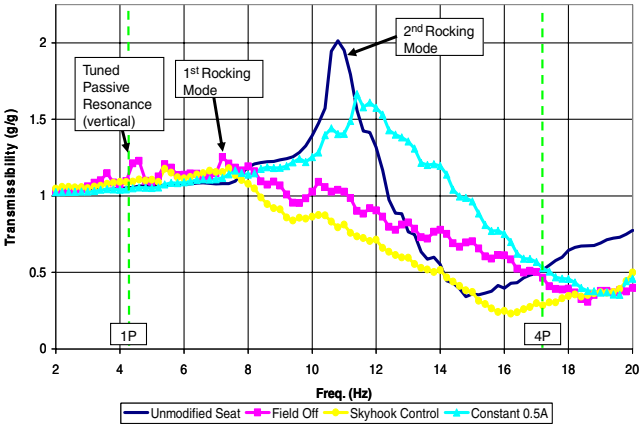

Fig. 19 Rear seat pan vertical transmissibility for 5th percentile female, 0.2 g excitation.

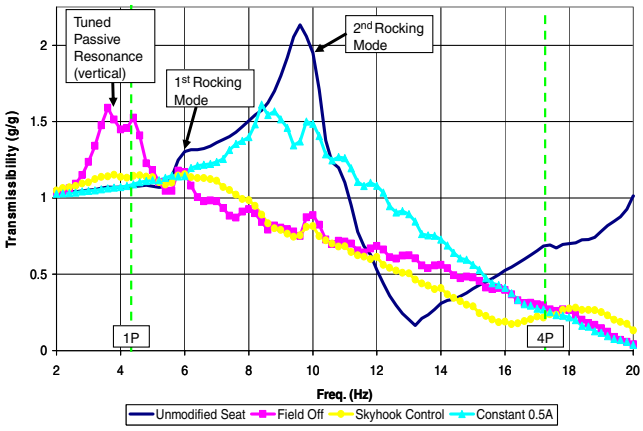

Fig. 20 Rear seat pan vertical transmissibility for 95th percentile male, 0.2 g excitation.

percentile female and a 0.2 g amplitude floor excitation. In this plot, not only have the resonant frequencies increased due to the lowered mass, but the tuned vertical resonance for the unenergized system is less pronounced. Additionally, the performance of the controlled system at the 4P frequency has worsened (71% attenuation of floor vibrations, 45% improvement over unmodified seat). These effects are likely due to the friction in the system that is not as easily overcome by the lowered inertial forces. Conversely, for a 95th percentile male occupant (Fig. 20), the tuned vertical resonance for the unenergized system is slightly more pronounced, and the performance of the controlled system at the 4P frequency has improved (78% attenuation of floor vibrations, 69% improvement over unmodified seat). This is again typical of friction in the system which is more easily overcome by the additional inertial force. As a final verification that friction was affecting system performance, the 50th percentile male occupant condition was tested at 0.4 g amplitude floor excitation. These results (Fig. 21) show much more pronounced tuned vertical resonance for the unenergized system and improved performance of the controlled system at the 4P frequency (85% attenuation of floor vibrations, 71% improvement over the unmodified seat). In this case, the additional inertial force provided by the increased excitation allows the friction to be more easily overcome, which improves performance.

Finally, the affect of the soft seat cushion was evaluated. The test results using a soft seat cushion under a 50th percentile occupant mass for a 0.2 g amplitude floor excitation are shown in Fig. 22. First, it can be seen that the rocking modes are much less significant, even for the unmodified seat. This is because the isolation provided by the seat cushion reduces the moment due to the CG offset and thereby reduces the amount of bending in the seat pan. The addition of the MR suspension, however, still provides an additional reduction in

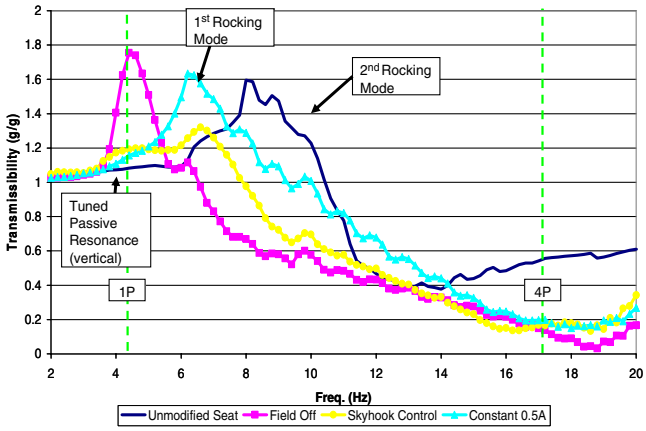

Fig. 21 Rear seat pan vertical transmissibility for 50th percentile male, 0.4 g excitation.

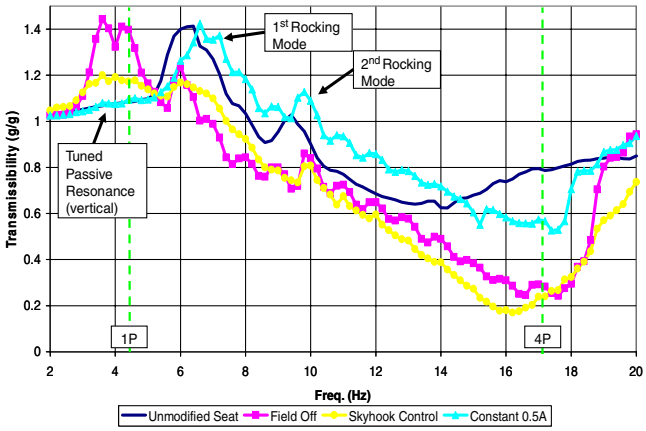

Fig. 22 Rear seat pan vertical transmissibility for 50th percentile male, 0.2 g excitation, with cushion.

these rocking modes. Additionally, the controlled system performance at the 4P frequency is maintained—76% attenuation of floor vibrations, which is a 70% improvement over the unmodified seat in this same condition.

Table 1 summarizes the key response reductions as compared to the unmodified SH-60 Seahawk crew seat. In general, it is shown that the vertical vibration isolation performance at the 4P increases with occupant weight and input excitation levels. As explained previously, this is likely due to friction in the system which is more easily overcome by a heavier occupant. Improved isolation of vertical 4P vibrations is also shown in the seat with a soft seat cushion, but the reductions in the rocking modes are less significant. As explained above, this is because the soft seat cushion provides some natural isolation to these rocking modes and the benefit of the suspension is less pronounced.

VIII. Conclusions

This study has explored the use of magnetorheological dampers in a semi-active seat suspension system for helicopter crew seats to enhance occupant comfort and reduce health issues resulting from whole body vibration. Key concepts in designing an MR seat suspension system to isolate the occupant from rotorcraft vibration were identified, and, using these design concepts, an MR damper was designed, fabricated, and retrofitted into a tactical SH-60 Seahawk crew seat. This MR damper was implemented in series with the FLEAs such that the crashworthiness capability of the seat was not impaired. A skyhook control algorithm was implemented and performance was evaluated both analytically and experimentally. Experimental test results have shown that this system reduced the dominant rotor-induced vertical vibration (4 per rev) transmitted to a 50th percentile male aviator by 76%, which is a 61–70% improvement over the unmodified SH-60 crew seat, depending upon whether a soft seat cushion is used. Furthermore, these experimental tests also show that this system significantly reduces vertically induced seat rocking that occurs as a result of an offset center of gravity in the crew seat design. This study has also shown that, although the dynamics of a tactical vehicle seat may be complex, a SDOF model can be a valuable tool for MR damper design and performance predictions.

Acknowledgments

This research was supported by the U.S. Naval Air Warfare Center Aircraft Division (Pax River, Maryland) under a Broad Agency Announcement (BAA) contract (N00421-06-C-0006) to Techno-Sciences, Inc. (Beltsville, Maryland) with William Glass as technical monitor. Additional research support was provided to N. M. Wereley under a grant from the Center for Rotorcraft Innovation (Rande Vause and Dan Good as technical monitors). Some instrumentation support was provided under a Defense University Research Instrumentation Program (DURIP) from the Army Research Office (Gary Anderson as technical monitor). The research team also wishes to recognize Armor Holdings for their collaboration in this research.

References

[1] Bonger, P. M., Hulshof, C. T. J., Dijkstra, L., Boshuizen, H. C., Groenhout, H. J. M., and Valken, E., "Back Pain and Exposure to Whole-Body Vibration in Helicopter Pilots," *Ergonomics*, Vol. 33, No. 8, 1990, pp. 1007–1026. doi:10.1080/00140139008925309

[2] Harrer, K. L., Yniguez, D., Majar, M., Ellenbecker, D., Estrada, N., and Geiger, M., "Whole Body Vibration Exposure for MH-60S Pilots" *Proceedings of the Forty Third Annual SAFE Association Symposium*, Safe Assoc., Creswell, OR, 24–26 Oct. 2005, pp. 303–314.

[3] Shanahan, D. F., Mastroiane, G., and Reading, T. D., "Back Discomfort in U.S. Army Military Helicopter Aircrew Member," *Backache and Back Discomfort*, AGARD, Neuilly-sur-Siene, France, AGARD-CP-378, Vol. 21, 1986, pp. 10–25.

[4] Hiemenz, G. J., Hu, W., and Wereley, N. M., "Investigation of MR Dampers for Enhanced Crashworthiness and Vibration Isolation of Helicopter Crew Seats," *Proceedings from the 63rd Annual AHS Forum*, American Helicopter Society, Alexandria, VA, May 2007.

[5] Choi, Y. T., and Wereley, N. M., "Biodynamic Response Mitigation to Shock Loads Using Magnetorheological Helicopter Crew Seat Suspensions," *Journal of Aircraft*, Vol. 42, No. 5, 2005, pp. 1288–1295.

[6] Desjardins, S. P., "The Evolution of Energy Absorption Systems for Crashworthy Helicopter Seats," *Journal of the American Helicopter Society*, Vol. 51, No. 2, 2006, pp. 150–163.

[7] Choi, S. B., Choi, J. H., Nam, M. H., Cheong, C. C., and Lee, H. G., "A Semi-Active Suspension Using ER Fluids for a Commercial Vehicle Seat," *Journal of Intelligent Material Systems and Structures*, Vol. 9, No. 8, 1998, pp. 601–606.

Table 1 Summary of key response reductions compared to unmodified SH-60 crew seat

Occupant/condition	5th percentile female, 0.2 g	50th percentile male, 0.2 g	95th percentile male, 0.2 g	50th percentile male, 0.4 g	50th percentile male w/cushion, 0.2 g
4P, vertical	45%	61%	69%	71%	70%
Seat rocking, longitudinal	93%	85%	88%	88%	46%
Seat rocking, vertical	82%	80%	82%	75%	25%
1P, vertical	−5%	−8%	−8%	−10%	−9%

[8] Choi, S. B., Nam, M. H., and Lee, B. K., "Vibration Control of a MR Seat Damper for Commercial Vehicles," *Journal of Intelligent Material Systems and Structures*, Vol. 11, No. 12, 2000, pp. 936–944.

[9] Park, C., and Jeon, D., "Semiactive Vibration Control of a Smart Seat with an MR Fluid Damper Considering Its Time Delay," *Journal of Intelligent Material Systems and Structures*, Vol. 13, Nos. 7–8, 2002, pp. 521–524.

[10] McManus, S. J., St. Clair, K. A., Boileau, P. É., Boutin, J., and Rakheja, S., "Evaluation of Vibration and Shock Attenuation Performance of a Suspension Seat with a Semi-Active Magnetorheological Fluid Damper," *Journal of Sound and Vibration*, Vol. 253, No. 1, 2002, pp. 313–327. doi:10.1006/jsvi.2001.4262

[11] Wereley, N. M., and Pang, L., "Nondimensional Analysis of Semi-Active Electrorheological and Magnetorheological Dampers Using Approximate Parallel Plate Models," *Smart Materials and Structures*, Vol. 7, No. 5, 1998, pp. 732–743. doi:10.1088/0964-1726/7/5/015

[12] Desjardins, S. P., Zimmerman, R. E., Bolukbasi, A. O., and Merritt, N. A., "Aircraft Crash Survival Design Guide," Aviation Applied Technology Directorate, USAAVSCOM, TR 89-D-22D, 1989.

[13] Gunston, T., and Griffin, M. J., "The Isolation Performance of a Suspension Seat Over a Range of Vibration Magnitudes Tested with an Anthropodynamic Dummy and Human Subjects," *Inter-Noise '99, Proceedings of the 28th International Congress and Exposition on Noise Control Engineering*, Multi-Science Publishing, Essex, U.K., Dec. 1999, pp. 949–954.

[14] Bousman, W. G., "Putting the Aero Back into Aeroelasticity," NASA/TM-2000-209589, USAAMCOM-TR-00-A-005, March 2000.

[15] Mao, M., Choi, Y.-T., and Wereley, N. M, "Effective Design Strategy for a Magneto-Rheological Damper Using a Nonlinear Flow Model," *Smart Structures and Materials 2005: Damping and Isolation*, SPIE, Bellingham, WA, Vol. 5760, pp. 446–455.

[16] Karnopp, D., Crosby, M., and Harwood, R., "Vibration Control Using Semi-Active Force Generators," *Journal of Engineering for Industry*, Vol. 96, No. 2, 1974, pp. 619–626.